Protein and Substrate Coordination to the Manganese Cluster in the Photosynthetic Water Oxidizing Complex: ^{15}N and ^{1}H ENDOR Spectroscopy of the S_2 State Multiline Signal in the Thermophilic Cyanobacterium *Synechococcus elongatus*[†,‡]

X.-S. Tang, M. Sivaraja, and G. C. Dismukes*

Contribution from Princeton University, Department of Chemistry, Hoyt Laboratory, Princeton, New Jersey 08544. *Received April 20, 1992*

Abstract: The hyperfine constants have been measured by ENDOR spectroscopy for ^{1}H and ^{15}N nuclei located within magnetic contact to the tetranuclear manganese cluster of the photosynthetic water oxidizing site in the thermophilic cyanobacterium *Synechococcus el.* The Mn cluster was examined in the S_2 oxidation state using the "multiline" EPR signal. The data were compared to model dimanganese(III,IV) complexes possessing both N and O ligand atoms and μ-oxo and μ-carboxylato bridging ligands. This revealed that the photosynthetic Mn cluster is coordinated predominantly by nonmagnetic O atoms having no covalently bound protons at α or β positions. This is indirect evidence for protein-derived carboxylato type ligands. Two ^{15}N hyperfine constants were resolved at 0.7 and 3.7 MHz. These values are comparable to the range predicted for coordination to π type sites on Mn^{III} or Mn^{IV} and exclude σ type coordination sites on Mn^{III} which yield much larger hyperfine constants. Either a single class of protein N (imidazole ?) ligands with coupling to both N1 and N3 atoms or possibly two coordination sites could be involved. An unexpectedly simple ^{1}H ENDOR spectrum was observed with two well resolved hyperfine splittings of 2.4 and 1.0 MHz and two poorly resolved or weak splittings of 4.9 and 0.5 MHz. All of these were removed by incubation in $^{2}H_2O$. Positive assignment to the Mn cluster was established by ENDOR-induced EPR. The ^{1}H ENDOR results differ greatly from those reported for the Mn cluster in spinach (Kawamori, Inui, Ono, Inoue *FEBS Lett.* **1989**, *254*, 219-224). The three largest splittings could be accounted for by a simple model involving a single rhombic ^{1}H tensor, with four possible sign choices for the principal values. One of these choices, $A_{x,y,z}$(dipolar) = -4.5, 2.9, 1.5 and A(isotropic) = -0.5 (MHz), coincided with the predicted dipolar and isotropic hyperfine terms obtained from a spin-coupled point-pair model used to describe the ligand dipolar hyperfine interaction with a pair of spin-coupled paramagnetic ions. The experimental ENDOR line shape could be approximately simulated by location of a proton nearly equidistant between the Mn ions along the normal to the Mn-Mn vector (R). The closest approach is predicted for the case of antiferromagnetically coupled Mn^{III} and Mn^{IV} ions, for which the proton would be located at R = 3.65 Å. At the present level of sensitivity, the hyperfine data suggest there may be no un-ionized water or hydroxo ligands directly bound to the Mn cluster but instead a "dry" environment with rather long (weak) H-bonds from solvent exchangeable protons to μ-oxo bridges or possibly to terminally coordinated ligands.

Introduction

Determination of the protein and substrate coordination structure of the four manganese ions comprising the photosynthetic water oxidase (WOC) and their association with a structurally required calcium ion is a goal which is hoped to reveal secrets about how this unique catalytic site activates water for dioxygen formation. Initial comparisons with redox-type dimanganese enzymes such as catalase[1] and (bacterial) ribonucleotide reductase has begun to reveal some structural and mechanistic similarities.[2]

Information on ligand coordination to the WOC has come from several kinds of experiments, including EPR, ENDOR, ESEEM, chemical modification of amino acid residues, and site-directed mutagenesis. An advantage of the magnetic resonance techniques is that one can make observations on the native enzyme without perturbing the metal binding site and so interpretation of the results is usually unambiguous. However, it requires isotopes with magnetic nuclei which interact with a paramagnetic center located within about 6-Å separation. On the other hand, mutagenesis and chemical modification techniques are potentially more sensitive to distant interactions mediated by conformational coupling, but require comparison of native with mutated or modified enzymes. A summary of the literature results follows.

The S_2 multiline EPR signal, arising from ^{55}Mn hyperfine structure in the mixed valence S_2 oxidation state of the tetramanganese cluster of the WOC, exhibits a nearly imperceptible line broadening upon exchange with ^{17}O-water, leaving unresolved the question of water coordination to the Mn cluster.[3a] Several groups have searched without success for line width narrowing of the S_2 multiline EPR signal upon exchanging water with $^{2}H_2O$, except for one claim which appears to involve changes other than those attributable to isotopic substitution alone.[3b] Deuterium ESEEM[4] and proton ENDOR[5] studies of the S_2 multiline EPR signal have found that $^{2}H_2O$ exchange leads to changes in these signals which are consistent with the presence of water or water exchangeable ligands near the Mn cluster. The ENDOR studies by Kawamori et al. provided structural information on six types of hydrogen atoms which were proposed to interact magnetically with the Mn cluster in spinach.[5] In our studies on the *Synechococcus elongatus* (formerly *Synechococcus sp.*) enzyme presented herein we find both quantitative and qualitative differences with the ENDOR results of Kawamori et al., suggesting the possibility of a striking difference in the atomic structure of

[†] Key terms: photosynthesis/water oxidation/manganese/ENDOR/^{15}N-label/S2-state multiline signal/water coordination/deuterium substitution.

[‡] Abbreviations: Chl, chlorophyll; DCBQ, 2,6-dichlorobenzoquinone; EDTA, ethylenediaminetetraacetic acid; ENDOR, electron-nuclear double resonance; ESEEM, electron spin echo envelope modulation; Mes, 4-morpholineethanesulfonic acid; PMSF, phenylmethanesulfonyl fluoride; PSII, photosystemII; WOC, water oxidizing complex.

(1) (a) Khangulov, S. V.; Varynin, V. V.; Melik-Adamyan, V. R.; Grebenko, A. I.; Voevodskay, N. V.; Blumenfeld, L. A.; Dobrykov, S. N.; Il'ysova, V. B. *Bioorgan. Khimiya* **1986**, *12*, 741-748 [Russ.]. (b) Khangulov, S. V.; Voevodskaya, N. V.; Barynin, V. V.; Grebenko, A. I.; Melik-Adamyyan, V. R. *Biofizika* **1987**, *32*, 1044-51 [Engl.]. (c) Fronko, R. M.; Penner-Hahn, J. E.; Bender, C. J. *J. Am. Chem. Soc.* **1988**, *110*, 7555.

(2) (a) Dismukes, G. C. In *Bioinorganic Catalysis*; Reedijk, J., Ed.; Marcel-Dekker, Amsterdam, 1993; pp 317-346. (b) Pecoraro, V. L. In *Manganese Redox Enzymes*; Pecoraro, V. L., Ed.; VCH Publ.: New York, 1992; Chapter 10.

(3) (a) Hansson, O.; Andreasson, L.-E.; Vanngard, T. *FEBS Lett.* **1986**, *195*, 151-154. (b) Nugent, J. H. A. *Biochim. Biophys. Acta* **1987**, *893*, 184-189.

(4) (a) Britt, R. D.; Zimmermann, J.-L.; Sauer, K.; Klein, M. P. *J. Am. Chem. Soc.* **1989**, *111*, 3522-3532. (b) DeRose, V. J.; Yachandra, V. K.; McDermott, A. E.; Britt, R. D.; Sauer, K.; Klein, M. P. *Biochem.* **1991**, *30*, 1335-1341. (c) Britt, R. d.; DeRose, V. J.; Yachandra, V. K.; Kim, D. H.; Sauer, K.; Klein, M. P. In *Curr. Prog. Photosyn. Res.* Baltscheffsky, M., Ed.; Kluwer Press: Dordrecht, 1990; Vol. 1, pp 769-772.

(5) Kawamori, A.; Inui, T.; Ono, T.; Inoue, Y. *FEBS Lett.* **1989**, *254*, 219-224.

0002-7863/93/1515-2382$04.00/0

the spinach and cyanobacterial enzymes which is not evident in their EPR spectra. In this paper we use both isotopic substitution with ^2H and ^{15}N, along with ENDOR-induced EPR (EIE) to assign and distinguish the hyperfine couplings for the S_2 multiline signal and Tyr-D$^+$. We also analyze the proton hyperfine interactions by simulation of the ENDOR line shape using a spin-coupled cluster model to describe the paramagnetic site and its interaction with magnetic ligands via both scalar and dipolar hyperfine couplings.

Evidence for binding of the substrate analog ammonia to the WOC was demonstrated via EPR spectral changes in the ^{55}Mn hyperfine structure of the S_2 multiline signal[6] and proven to be a direct ligand to Mn by ESEEM measurements.[4a] Binding was found to occur in the S_2 state and to require a structural rearrangement.[6a,b] On the basis of the ESEEM detected ^{14}N nuclear quadrupole splitting, the binding site was suggested to involve proton ionization to form a μ-amino bridge between Mn ions, Mn–NH_2–Mn.[4a] It was hypothesized that this may correspond to a water binding site.

A small but undetermined number of a single type of protein derived N atoms has been implicated as magnetically interacting with the Mn cluster on the basis of ESEEM studies of ^{14}N coupling in the cyanobacterium *Synechococcus el.*[4b,c] Although the ^{14}N ESEEM resonance disappeared upon cell growth in ^{15}N media, the expected signal from the ^{15}N isotope was not observed, and determination of the ^{14}N hyperfine and quadrupole couplings was not reported. The chemical origin of the amino acid was not established, and it was unclear if it was a direct ligand to the Mn cluster or perhaps only involved in H-bonding to a first shell donor ligand. This result was insightful because it indicated that the majority of weakly interacting ligand atoms were not N and thus must come from nonmagnetic, i.e., oxygen, ligands. This result was hinted at previously by EPR data showing that the ^{15}N isotopic substitution failed to produce an observable change in the substructure or line width of the S_2 multiline signal.[4b,7] Unfortunately, the ESEEM method is unable to resolve hyperfine interactions to all magnetic ligands. Particularly troublesome to observe are strongly coupled nuclei (hyperfine $\gg$ nuclear Zeeman) and those having no quadrupole moment (^{15}N, ^1H). Thus the most strongly coupled ^{14}N nuclei in the mixed valence cation, $[(bpy)_2Mn^{III}(\mu\text{-}O)_2Mn^{IV}(bpy)_2]^{3+}$, give a hyperfine constant detected by ENDOR of 7.6 MHz (if the quadrupole constant is taken as 3.0 MHz) which is absent in the X-band ESEEM. Accordingly, ENDOR studies of the PSII WOC can yield new insights into the ligand coordination of the Mn cluster.

Histidine has been proposed to function as a redox active residue to mediate charge transfer between the Mn cluster and Tyr-Z$^+$ (reaction center D1 polypeptide residue Tyr-161).[8] This proposal received support from the results of Tamura et al. demonstrating that N-alkylation of histidines with diethyl pyrocarbonate (DEPC) leads to loss of Mn photoligathion in Mn-depleted PSII membranes.[9] On the basis of chemical modification and protease cleavage studies both histidine and carboxylate residues (Asp and Glu) have been implicated as important for reassembly of the Mn cluster and recovery of water oxidation.[10] Rebinding of the two more loosely bound Mn ions out of the four is suppressed by chemical modification of carboxyl residues but not histidine. Furthermore, it was found that the high affinity Mn ligation site, which is blocked in the Scenedesmus LF-1 mutant possessing an unprocessed carboxyl terminus of the D1 reaction center subunit (nine additional residues), could be a histidine residue on the basis that DEPC can block Mn binding to this site following removal of the carboxyl terminus with proteases.[11] Chemical modification with DEPC also suppresses the capacity for photoactivation, the recovery of O_2 evolution is depleted PSII membranes by light and inorganic cofactors, and alters thermoluminescence attributed to histidine photooxidation.[12]

Site-directed mutagenesis of the transformable cyanobacterium *Synechocystis* 6803 has provided indirect evidence for the possible involvement of two residues in water oxidation. Nixon and Diner have given evidence that Asp170 of the D1 reaction center subunit is required for the binding or stabilization of Mn on the basis of loss of electron donation to Tyr-Z$^+$ in the Asp170Ser mutant.[13] Vermaas et al. have shown on the basis of steady-state O_2 evolution rates that Glu69 of the D2 reaction center subunit is required for stable O_2 activity.[14] These results are noteworthy because they suggest that apparently distant residues on both the D1 and D2 reaction center subunits are implicated in stabilizing the WOC.

A summary of the published data in the form of a model for the ligand coordination to the Mn cluster remains largely incomplete. However, it appears that the ligand types are dominated by O donor atoms which stabilize the Mn^{III} oxidation state vs Mn^{II} (Asp and Glu). At least one N donor residue, possibly histidine, comprising a single class of magnetically indistinguishable N atoms may be involved either as direct ligands to Mn or H-bonded to Mn ligands. An amino acid located within 9 Å to the WOC is rendered photooxidizable upon removing either calcium[15,16] or by substituting Cl^- with F^- in the WOC.[17] Although the identity of the amino acid remains uncertain, the electronic spectrum of the radical suggests that it could arise from histidine.[18] This limited picture suggests a coordination structure which appears to be similar to that found in binuclear redox enzymes like manganese catalase and ribonucleotide reductase, but unlike that in dioxygen binding enzymes like hemerythrin and hemocyanin.[2a]

In the present study, we show that it is possible to observe two classes of nitrogen atoms which are in magnetic contact with the Mn cluster and obtain their hyperfine coupling constants. Also, hydrogen atoms derived from water exchangeable protons bound to the active site of the Mn cluster are resolved and their distance of separation assigned using a quantum mechanically correct description of the electron spin distribution for a mixed valence dimanganese site coupled via the Heisenberg exchange interaction and exhibiting no Mn-ligand spin transfer.

Experimental Methods

Cells of the thermophilic cyanobacterium *Synechococcus el.* were grown for 2–3 days at 52–54 °C in 20 L using the modified medium of Dyer and Gafford as described by Katoh.[19] The culture (0.5 × 4 ft chamber) was continuously illuminated with fluorescent lamps (6 × 34 W each) and bubbled with air enriched with approximately 5% carbon dioxide. For ^{15}N experiments, 99.9% [^{15}N]-nitrate was used as the sole N source during cell growth.

Oxygen-evolving PSII complexes were prepared from *Synechococcus* thylakoid membranes according to the method described by Katoh.[19] The PSII preparations typically have O_2 evolving activities of 2–3 mmol O_2/mg chl/h at 40 °C and pH 6.5 with 0.4 mM DCBQ as electron

(6) (a) Beck, W. F.; dePaula, J. C.; Brudvig, G. W. *J. Am. Chem. Soc.* **1986**, *108*, 4018–4022. (b) Beck, W. F.; Brudvig, G. W. *Biochemistry* **1986**, *25*, 6479–6486. (c) Aasa, R.; Andeasson, L.-E.; Lagenfelt, G.; Vanngard, T. *FEBS Lett.* **1987**, *221*, 245–248. (d) Andreasson, L.-E.; Hansson, O.; Von Schenck, K. *Biochim. Biophys. Acta* **1988**, *936*, 351–360.

(7) Andreasson, L.-E. *Biochim. Biophys. Acta* **1989**, *973*, 465–467.

(8) Kanbara, T.; Govindjee *Proc. Natl. Acad. Sci. U.S.A.* **1985**, *581*, 228–236.

(9) Tamura, N.; Ikeuchi, M.; Inoue, Y. *Biochim. Biophys. Acta* **1989**, *973*, 281–189.

(10) (a) Seibert, M.; Tamura, N.; Inoue, Y. *Biochim. Biophys. Acta* **1989**, *974*, 185–191. (b) Preston, C.; Seibert, M. *Biochemistry* **1991**, *30*, 9615–9624. (c) Preston, C.; Seibert, M. *Biochemistry* **1991**, *30*, 9625–9633.

(11) Preston, C.; Seibert, M. *Photosyn. Res.* **1989**, *30*, 101–113.

(12) Ono, T.-A. and Inoue, Y.; *FEBS Lett.* **1991**, *278*, 2, 183–186.

(13) Nixon, P. J.; Diner, B. A. Proc. 17th IEEE: Engineering in Medicine and Biology Society Pedersen, P. C., Onaral, B., Eds.; 1990; pp 1732–1734.

(14) Vermaas, W. F. J.; Charite, J.; Shen, G. *Biochemistry* **1990**, *29*, 5325–5332.

(15) Boussac, A.; Zimmermann, J.-L.; Rutherford, A. W. *Biochemistry* **1989**, *28*, 8984–8989.

(16) (a) Sivaraja, M.; Tso, J.; Dismukes, G. C. *Biochemistry* **1989** *28*, 9459–9464. (b) Tso, J.; Sivaraja, M.; Dismukes, G. C. *Biochemistry* **1991** *30*, 4734–4739. (c) Tso, J.; Sivaraja, M.; Philo, J. S.; Dismukes, G. C. *Biochemistry* **1991**, *30*, 4740–4747.

(17) Baumgarten, M.; Philo, J. S.; Dismukes, G. C. *Biochemistry* **1990**, *29*, 10814–10822.

(18) (a) Boussac, A.; Zimmermanm, J.-L.; Rutherford, A. W. *FEBS Lett.* **1990**, *277*, 69–74. (b) Boussac, A.; Zimmermann, J.-L.; Rutherford, A. W. *Biochemistry* **1989**, *28*, 8984–8989. (c) Boussac, A.; Zimmermann, J.-L.; Rutherford, A. W.; Lavergne, J. *Nature* **1990**, *347*, 303–306.

(19) Katoh, S. *Methods Enzymol.* **1988**, *167*, 263–269.

acceptor measured with a Clark-type oxygen electrode. Prior to ENDOR measurements PSII complexes were suspended in 10% (w/v) glycerol buffer containing 50 mM Mes-NaOH (pH 6.5), 5 mM $CaCl_2$, 10 mM NaCl, 0.5 mM PMSF, and centrifuged at 4 °C and 300000 g for 2 h. The pellet was then resuspended in 50% (w/v) glycerol buffer containing 50 mM Mes-NaOH (pH 6.5), 5 mM $CaCl_2$, 10 mM NaCl, 1 mM DCBQ and 1 mM EDTA. For exchange against ^2H_2O, samples were suspended in ^2H_2O containing 10% (w/v) deuterated glycerol ($C_3H_5O_3{}^2H_3$) buffer prepared from ^2H_2O. The concentration of PSII was adjusted to 50 μg chl/mL, and the sample was illuminated under room light at 25 °C for 30 min. The PSII particles were then collected by ultracentrifugation and resuspended in 50% glycerol buffer as described before, except using deuterated glycerol and ^2H_2O. PSII samples at 3–4 mg chl/mL were loaded into EPR tubes, dark-adapted at 4 °C for 30 min, and frozen in liquid N_2 in darkness. To form the S_2 state multiline signal, samples were illuminated at 210 K for 15 min using a water-filtered 300 W tungsten lamp, followed by dark-adaptation for 1 min at 250 K to reoxidize Q_A^- and refrozen to 77 K. This thermal cycling eliminated the EPR signal for Q_A^- which is reoxidized and might have otherwise interfered with the ENDOR studies. A broad light insensitive baseline signal centered at g 2 was present in the dark treated samples. The area of this signal is 1/3 to 1/4 of the light induced area. There is no evidence for light sensitivity of this baseline EPR signal in Tris treated PSII samples devoid of manganese.

EPR spectra were recorded with a Bruker ESP-300 spectrometer at temperatures above 4.2 K using an Oxford Instruments ESR-900 continuous flow cryostat.[16] ENDOR spectra were recorded at 9.45 GHz using a Bruker ESP300/ER250A EPR/ENDOR spectrometer operating with a TM110 microwave cavity fitted with a 1–30 MHz coil mounted on a quartz dewar flask (Bruker). An Oxford ESR910 immersible liquid helium cryostat was used for all ENDOR studies. Typically, ENDOR measurements were performed at a temperature yielding a maximum vapor pressure of 22 mm, corresponding to T = 2.1 K. ENDOR spectra were recorded in the absorption EPR mode at an optimized microwave power. The line shape of the experimental ENDOR data were usually asymmetric with the lower Zeeman component of different intensity than the upper Zeeman component for each proton. The reasons for this stem in a complex was on several different relaxation pathways for the ENDOR effect, rather than a limitation of the instrumentation.[20]

Many attempts were made to obtain ENDOR data using a gaseous helium cryostat which achieved a base temperature of 4.2–5.5 K prior to rf excitation. In all cases, the spectra were not reproducible (Baumgarten, M. unpublished results). We found that to observe ENDOR from the S_2 multiline signal it was essential to perform measurements in liquid helium below 4.2 K and preferably below 2.1 K under highly stable temperatures over the course of the integration times (~7 h).

Results

EPR. We chose to perform our studies using PSII membranes from the thermophilic cyanobacterium *Synechococcus el.* rather than the more common spinach source because it is easy to grow cells on ^{15}N-nitrate to achieve isotopic enrichment, and because it produces an intense S_2 multiline EPR signal essential for ENDOR studies. PSII membranes were observed to have negligible PSI and cyt b_6/f contamination as seen by the lack of $P700^+$ and Rieske FeS EPR signals produced by illumination or in the dark, respectively (<5%). The baseline signal also revealed a light insensitive Cu^{2+} signal at g = 2.05 and cyt b559 at g = 2.2. The light induced S_2 state signal had an integrated area equal to 3–4 times the area of the underlying dark baseline signal. To obtain the maximum intensity of the S_2 multiline EPR signal in PSII membranes of *Synechococcus el.* it is essential that glycerol be present in the final suspension medium (>30%). This is similar to the situation for spinach where the EPR microwave saturation characteristics of the S_2 multiline signal depend on the cryoprotectant used (sucrose, ethylene glycol, etc.). Figure 1A presents a typical light-dark difference spectrum of the S_2 multiline EPR signal used for ENDOR measurements. The sharp central radical signal at g 2 corresponds to the minor fraction of Tyr-D^+ radical which is light-induced. The arrows indicate three magnetic field positions at which ENDOR measurements were typically performed. Curves 1 and 2 of Figure 1B are an expansion of the four peaks at the high field end for samples grown on natural abundance nitrate (curve 1) vs 99.9% ^{15}N-nitrate (curve 2) as the sole N source. No observable change in the multiline signal substructure was detected, indicating that the line width is determined predominantly by factors other than ^{14}N hyperfine structure. This is in agreement with previous studies.[4b]

(20) Scholes, C. P. In *Multiple Electron Resonance Spectroscopy*; Dorio, M. M., Freed, J. H., Eds.; Plenum Press: New York, 1979; Chapter 8.

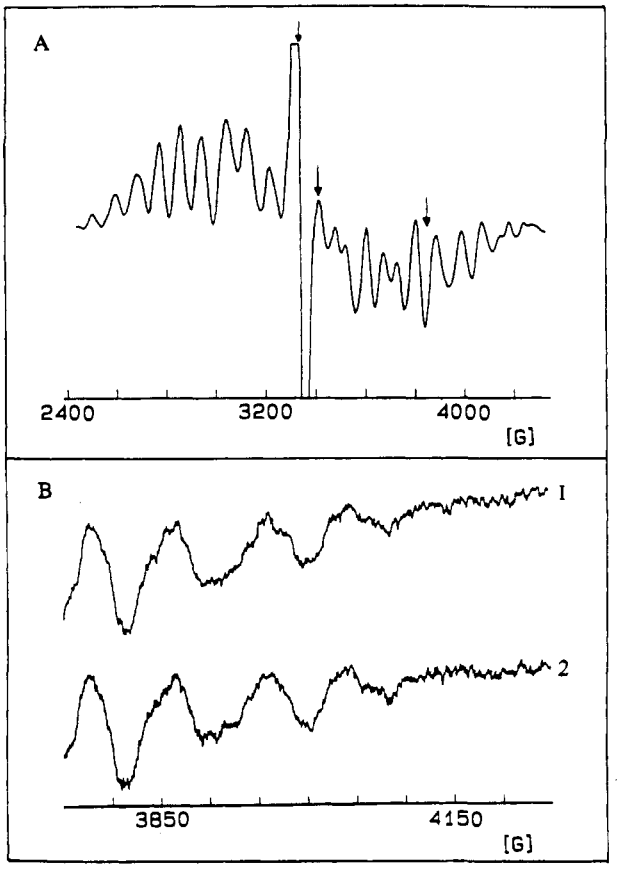

Figure 1. (A) Light-minus-dark EPR difference spectrum of the S_2 multiline signal in PSII particles from *Synechococcus el.* EPR conditions: temperature, 10 K; microwave power, 32 mW; number of scan, 1; time constant, 80 ms; 20 G modulation at 100 kHz. Arrows indicate the magnetic field for ENDOR experiments. (B) EPR spectra comparing the multiline substructure in PSII particles from *Synechococcus el.* grown on ^{14}N (curve 1) and ^{15}N (curve 2). EPR conditions: microwave power, 12.8 mW; number of scans, 25; 5 G modulation at 100 kHz.

Table I. Hyperfine Constants (MHz) from ^{15}N ENDOR and ESEEM of the S_2 Multiline EPR Signal in PSII WOC Particles

PSII	A (^{15}N)	method	ref
S_2	3.7, 0.7	ENDOR	this work
S_2	not detected[a]	ESEEM	Britt et al.[4b,c]
S_2-NH_3	3.2	ESEEM	Britt et al.[4a]

[a] ^{14}N absorption was observed at 4.8 MHz.

^{15}N ENDOR of PSII. Figure 2A,B shows that samples grown on [^{15}N]-nitrate gave three strong signals between 1 and 4 MHz which were absent in samples grown on [^{14}N]-nitrate (C). This is expected since the lack of the (anisotropic) quadrupole moment for ^{15}N leads to much sharper and fewer lines. These signals were induced by the illumination/annealing procedure and are presented as light-minus-dark difference spectra. The magnetic field dependence of the ENDOR peaks was followed by performing measurements at several of the peaks of the multiline EPR signal; Figure 2 shows ENDOR data at 3416 and 3838 G. This was consistent with a magnetic moment attributable to ^{15}N as the source.

The ENDOR spectrum for each ^{15}N nucleus is expected to consist of a pair of lines at resonance frequencies given by eq 1.

$$\nu = |A/2 \pm \nu_n| \quad (1)$$

When the hyperfine constant, A, is larger than the nuclear Zeeman frequency, ν_n, the spectrum is centered at $A/2$ and split by $2\nu_n$.

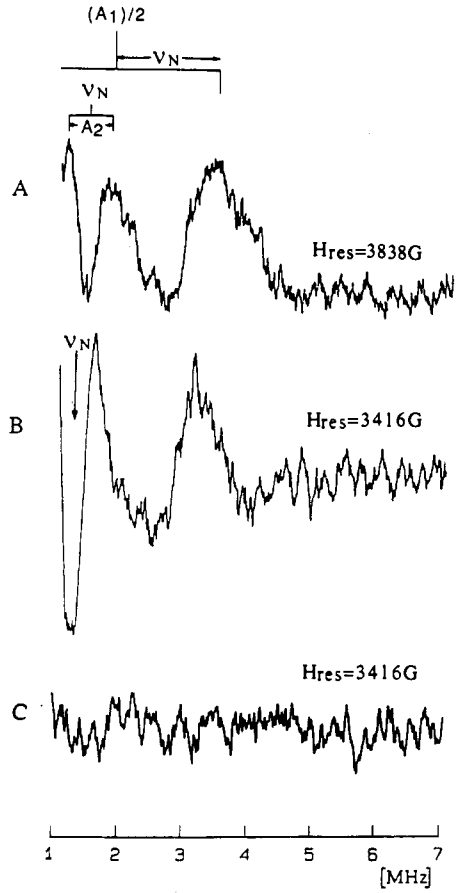

Figure 2. (A) and (B) show light-minus-dark ENDOR spectra from the S_2 multiline signal from PSII preparations of *Synechococcus el.* Cells were grown on [^{15}N]-nitrate as the sole source of nitrogen. (C) The same as (B) except using ^{14}N grown cells. Spectra were recorded at two magnetic fields 3416 G (B and C) and 3838 G (A). Instrumental conditions: microwave frequency: 9.44 GHz; microwave power: 20 mW; modulation frequency: 12.5 kHz; FM depth: 99.76 kHz; maximum RF power 100 W; temperature: 2.1 K; time constant, 80 ms; number of scans, 600 (for A) and 300 (for B and C).

This is the situation which applies to the highest frequency peak at 3.2–3.4 MHz. It is associated with a lower frequency component which falls below the 1 MHz cut-off of our spectrometer. Using ν_n = 1.47 MHz at 3416 G, we obtain A_1 = 3.7 MHz. For the peak at 1.8 MHz we have $\nu_n > A_2$, so that the doublet is centered at the nuclear Zeeman frequency and split by A; one obtains A_2 = 0.7 MHz. These hyperfine constants are listed in Table I.

^{1}H ENDOR of PSII. Figure 3A–C gives the ENDOR spectrum between 10 and 20 MHz of PSII samples recorded at an EPR magnetic field of 3415 G in the light (A), dark (B), and the difference spectrum (C). Because of the presence of a light-insensitive broad background EPR signal present in dark adapted (S_1) samples and underlying the light-induced S_2 multiline signal it is important that ENDOR experiments be recorded as difference spectra. These data were obtained on samples immersed in liquid helium at 2.1 K.

The light-dark difference spectrum reveals three pairs of splittings at 4.9, 2.3, and 1.0 MHz, in addition to the unresolved matrix peak centered on the free proton Zeeman frequency. Subtraction of a gaussian function of equal line width to the matrix peak from the experimental spectrum revealed the spectrum in Figure 5, from which another hyperfine splitting of 0.5 MHz may be resolved. Other minor features were not sufficiently strong or reproducible to identify. All three pairs of splittings and the light-induced matrix peak disappeared in samples that were exchanged with ^2H_2O under illumination, as described in the Experimental Section. The magnetic field dependence of these peaks was determined at the field positions noted in Figure 1 and was in agreement with the magnetic moment of the proton.

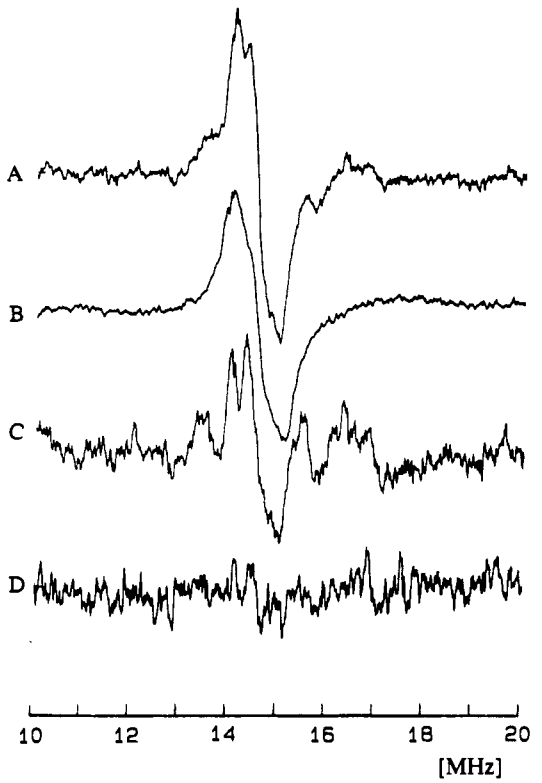

Figure 3. ^{1}H ENDOR spectra of *Synechococcus el.* PSII particles, (A) illuminated sample, (B) dark adapted sample, and (C) light-minus-dark difference spectrum (A-minus-B). (D) Light-minus-dark spectrum of PSII particles exchanged with ^2H_2O as described in the text. Instrumental conditions: magnetic field, 3415 G; microwave power, 10 mW; number of scans; 400 (for A–C) and 200 (for D). For details see Figure 2.

To investigate further the origin of these signals we performed the ENDOR-induced-EPR experiment in which the magnetic field and rf frequency are swept together so as to maintian constant resonance excitation of the proton ENDOR peak of interest.[21] Figure 4A curve 1 illustrates again the proton ENDOR region of PSII obtained at a fixed magnetic field. Figure 4A curve 2 gives the proton ENDOR signal from Tyr-D$^+$ obtained in the dark at 3355 G. Above curve 1 are four arrows denoting the four rf frequencies at which EIE was examined. They correspond to the central matrix peak (a), the 2.4 MHz resonance (b), the 4.0 MHz resonance from Tyr-D$^+$ (c) and off resonance at 6.0 MHz (d). The EIE spectra at these four rf frequencies are given in Figure 4Ba–d. They are compared to the integral of the S_2 multiline EPR signal given in Figure 4Be. These data show clearly that the light-induced matrix ENDOR peak at ν_H arises from two EPR signals having line shapes and g factors which resemble those of Tyr-D$^+$ and the S_2 multiline signal. The full line width at half-maximum of the integrated light-induced EPR signal is 750 G, while the EIE line width is about 600 G. The line widths of EPR and EIE signals are not necessarily the same, nor are they simply related. The resonance at 2.4 MHz comes from an EPR signal having a broad line shape and g value similar to the S_2 multiline signal, while the 4.0 MHz resonance originates from an EPR signal having a line shape and g factor the same as Tyr-D$^+$. No EIE signal was observed when the rf frequency was maintained off resonance. Based on these studies it was possible to assign the light-induced resonances at 1.0 and 2.4 MHz to a light-induced EPR signal with line shape similar to the S_2 multiline signal. The resonances at 0.5 and 5.0 MHz were not strong enough to perform the EIE experiment. However, because these are light-induced and absent in the dark Tyr-D$^+$ ENDOR spectrum we could assign them to the S_2 oxidation state. Weakly coupled

(21) Kurreck, H.; Kirste, B.; Lubitz, W. *Electron Nuclear Double Resonance Spectroscopy of Radicals in Solution*; VCH Publishers: New York, 1988; p 41.

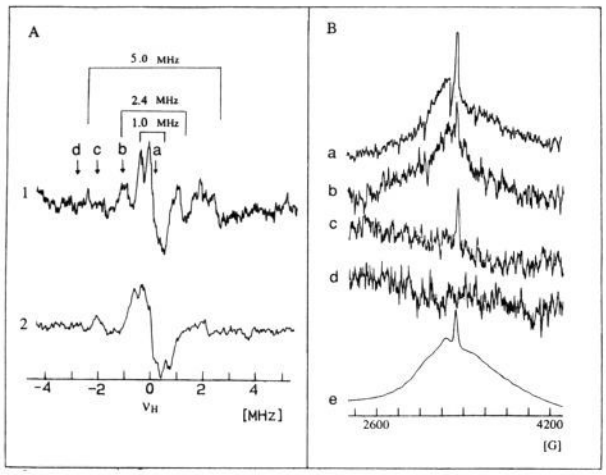

Figure 4. (A) Comparison of the ENDOR spectra of the S_2 multiline state (light-minus-dark) (curve 1) versus dark Tyr-D$^+$ ENDOR signal (curve 2). Arrows indicate the RF position for ENDOR-induced-EPR (EIE). Number of scans, 400 (curve 1) and 10 (curve 2). (B) (a–d) show EIE signals for an illuminated PSII sample at different RF frequency as shown in (A). (Be) shows the EPR absorption spectrum for the same sample: number of scans, 100. For details see Figure 3.

Table II. ^{1}H ENDOR Hyperfine Constants (MHz) in PSII Particles

signal origin	peak position a	b	c	d	e	f	g	ref
S_2-state	0.5[a]		1.0[a]		2.4[a]	4.9[a]		this work
multiline signal	0.53[b]	0.76[b]	1.19[b]	1.44[b]	2.41[a]	4.01[a]		5
Tyr-D$^+$ signal		0.75		1.38		4.11	7.64	29

[a] ^2H_2O exchangeable. [b] ^2H_2O nonexchangeable.

protons which exhibit hyperfine couplings at or less than the matrix peak line width of 0.35 MHz contribute to ENDOR from both the Tyr-D$^+$ and the S_2 multiline signals. Table II summarizes these assignments.

Discussion

^{15}N ENDOR. The data of Figure 2 and Table I demonstrate that there are two ^{15}N hyperfine constants of 3.7 and 0.7 MHz arising from ligands to the WOC in the S_2 state. We favor the interpretation that these are due to two different N atoms, rather than to a single atom possessing a highly anisotropic hyperfine tensor, for two reasons. The ENDOR resonances are of equal intensity without the expected powder line shape for an anisotropic tensor. Nor is there precedent to support the occurrence of such large hyperfine anisotropy for N bound to transition ions having either σ or π type spin density.[24,25] Previous evidence for hyperfine coupling between the PSII Mn cluster and a single class of ^{14}N atoms was obtained from ESEEM studies of this same enzyme, although neither the hyperfine nor the quadrupole coupling constants were determined.[4b,c]

To judge if these could be attributable to amino, amide, or aromatic (imidazole) N ligands coordinated to Mn^{III} and Mn^{IV} requires comparison to model complexes. Table III summarizes the literature we have found for the ^{14}N hyperfine and quadrupole

Table III. ^{14}N ENDOR and ESEEM of $N_4Mn^{III}(\mu\text{-}O)_2Mn^{IV}N_4$ Complexes and Catalase

terminal ligand	coordination type		$\lvert A\rvert$ (MHz)	$\lvert Q_{zz}\rvert$ (MHz)	method	ref
$[L_2Mn^{III}(\mu\text{-}O)_2\text{-}Mn^{IV}L_2]^{3+}$						
L = bpy	σ	A_1	11.4	3.0	ENDOR	23
	π	A2-A4	1–5	nd		
	π	A	2.8	2.3	ESEEM	4b,c
L_2 = cyclam	σ	A_1	9.2	3.0	ENDOR	24
	π	A_2-A_4	1–4	nd		
L_2 = tmpa	σ	A_1	11.2	3.0	ENDOR	24
	π	A_2-A_4	2–5	nd		
catalase (*thermus th.*)	π	A	2.3	2.44	ESEEM	27

coupling constants ($|Q_{zz}|$) for dimanganese(III,IV) complexes and the catalase enzyme from *Thermus thermophilus*. This reveals that for valence trapped di-μ-oxo complexes two classes of hyperfine constants have been observed for terminally coordinated pyridine, secondary amine, and bipyridine ligands. A large value in the range of 7.6–11.4 MHz and more than one smaller hyperfine constants in the range 1–5 MHz were detected by ENDOR. A single hyperfine constant in the range 2.3–2.8 MHz has also been observed by ESEEM for some of these complexes. These two classes appear to represent the cis and trans coordination sites with respect to the Mn_2O_2 plane, respectively; there are four nonequivalent terminal sites, two on each Mn ion which are cis(2) or trans(2) with respect to the Mn_2O_2 plane. The larger hyperfine constant is expected for the N ligand coordinated to the Mn^{III} ion (electron configuration $d_\pi^3 d\sigma^1$) and directed toward the orbital bearing the single antibonding d_σ electron; this site corresponds to the cis position as determined by X-ray crystallography (see structure **1**). Hence, we call this a σ site. N donors at the two

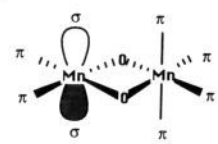

1

trans sites on Mn^{III} and all sites on Mn^{IV} have only π symmetry interactions with the unpaired electrons on their respective Mn ions, which are expected to give much smaller hyperfine couplings. The smaller hyperfine constants in the range 1–5 MHz reported in Table III can be attributed to π type coordination sites. This classification also holds true for the ^{14}N quadrupole constants; a larger value, about 3.0 MHz, is associated with the σ type site, while a smaller value, about 2.3–2.4 MHz, is associated with the π type site. A reduction in both Q_{zz} and $a_{iso}(^{14}N)$ for the π type N-1 imidazole atom in $Fe^{III}(TPP)(Im)_2^+$ vs the σ type N-1 imidazole atom in high-spin aquometmyoglobin has been reported: –0.8 and 5.6 MHz vs –1.12 and 9.3 MHz, respectively.[25] The smaller Q_{zz} for π type N donors has been rationalized as due to the stronger metal–N bonding and the attendant lowering in asymmetry of the electron density around N.

From this analysis we can conclude that there appear to be no σ type N ligands bound to the manganese cluster in PSII. The observed PSII ^{15}N hyperfine cosntants of 3.7 and 0.7 MHz correspond to expected ^{14}N hyperfine constants of 2.6 and 0.5 MHz, respectively. The larger of these two falls in the range reported for the weakly coupled class of terminally coordinated amino and aromatic N atoms to $Mn_2O_2^{3+}$ cores and also the lone N coupled to the Mn^{III}Mn^{IV} core of manganese catalase, as given in Table III. We ascribe the 3.7 MHz coupling to a N atom coordinated directly to a π type site on Mn^{III} or any position on Mn^{IV}, as described below. It is unclear if the smaller value of 0.5 MHz falls in this same class or perhaps in a new class of very weakly coupled N atoms which are not directly coordinated to Mn.

Although there are no literature reports of the hyperfine constants for the two N atoms of imidazole when bound to Mn^{III} or Mn^{IV}, we can estimate what they should be from other metal–

(22) Baumgarten, M.; Sheats, J. E.; Dismukes, G. C. to be published.
(23) (a) Dismukes, G. C.; Tang, X.-S.; Khangulov, S.; Sivaraja, M.; Pessiki, P.; Barynin, V. V.; *Proceedings of the 9th International Congress on Photosynthesis*; Murata, N., Ed.; Kluwer Acad. Press: Dordrecht; pp 257–264. (b) Khangulov, S.; Barynin, V.; Dismukes, G. C. *Biochemistry*, in press.
(24) Tan, X.-L.; Gultneh, Y.; Sarneski, J. E.; Scholes, C. P. *J. Am. Chem. Soc.* **1991**, *113*, 7853–7858.
(25) (a) Scholes, C. P.; Falkowski, K.; Chen, S.; Bank, J. *J. Am. Chem. Soc.* **1986**, *108*, 1660–1671. (b) Scholes, C. P.; Lapidot, A.; Mascarenhas, R.; Inubushi, T.; Isaacson, R. A.; Feher, G. *J. Am. Chem. Soc.* **1982**, *104*, 2724–2735.

imidazole complexes. The literature values for the ^{14}N-1 and ^{14}N-3 hyperfine constants of imidazole coordinated to Cu^{II} are 40 and 1.5 MHz (ratio 27/1), respectively. These refer to a square planar type complex with a $d_{x^2-y^2}$ ground state and hence the unpaired spin density is directed toward the imidazole ligand in a σ type orbital. We can predict the ^{14}N hyperfine constant this would have to Mn^{III} as follows. If the hyperfine constant is due predominantly to the Fermi contact interaction and the unpaired electron spin density remains mostly on the metal, then the spin density can be obtained by dividing by 2 S_Z. For Mn^{III} this is 4, hence the predicted Fermi contact hyperfine constant should be about 10 MHz for imidazole N coordinated at a σ site to Mn^{III}. This is very close to the observed range for the σ type coordinated N ligands to Mn^{III}, 7.6–11.4 MHz, as noted in Table III. This is our basis for assignment of this large hyperfine constant to σ type N ligands. By the same reasoning, the ^{14}N-3 imidazole Fermi contact hyperfine constant is predicted to be at 1.5/4 or about 0.4 MHz. Since this cannot exist without the larger N-1 coupling, we may exclude this assignment for Mn catalase.

For π type imidazoles in low spin $Fe^{III}(TPP)_2(Im)_2^+$ the ^{14}N-1 hyperfine is 5.6 MHz, while N-3 was not detected.[25] Thus the predicted hyperfine constant for imidazole N-1 bound to a π site on Mn^{III} should be about 5.6/4 or about 1.4 MHz. Likewise, for Mn^{IV} it should be about 5.6/3 or about 1.9 MHz. These approximate values fall in the low end of the range for the observed hyperfine constants for directly coordinated N ligands bound to Mn^{III} and Mn^{IV}, as given in Table III. This is our basis for assigning these to π type coordination sites. A value for the N-3 hyperfine constant has not been reported for a π type imidazole where N-1 is also known. However, low-spin cytochrome P450 has been estimated to have a N-3 hyperfine constant of 1.8 MHz.[30] Using the typical N-1 hyperfine of 5.1–5.6 for low-spin Fe^{III} complexes[25,31] as an approximation for cytochrome P450 gives a hyperfine ratio of 3 for N-1/N-3 for π type imidazole. This leads to predicted π type ^{14}N-3 hyperfine constants of 0.5 MHz for Mn^{III} and 0.6 MHz for Mn^{IV}. Both the experimental correlations noted in Table III and the theoretical extrapolations given here lead to the interesting possibility that the two experimentally determined N hyperfine constants for PSII are consistent with the N-1 and N-3 hyperfine constants for π type imidazoles coordinated to Mn^{III} or Mn^{IV}. The hyperfine constants predicted above should be further scaled in magnitude by a factor of $(S_i \cdot S)/S^2$ for N ligands bound to a spin-coupled dimanganese-(III,IV) center, as discussed below.

Are the two N hyperfine constants due to two separate protein residues bound to the first coordination shell, or could they be due to the two N atoms of a single imidazole ligand, as suggested in the preceding paragraph? This is difficult to judge on the basis of hyperfine constants alone because it is possible for chemically equivalent ligands to exhibit different hyperfine constants when bound to inequivalent Mn ions in a spin coupled cluster. Thus, the well-known doubling of the $^{55}Mn^{III}$ hyperfine constant, relative to the monomer value, in spin coupled $Mn^{III}Mn^{IV}$ complexes also applies to the ligands coordinated to it.[26] This means that we cannot distinguish between these two cases with the present information. Our results are consistent with the hypothesis based on chemical modification studies that two histidines could be involved in coordination or stabilization of the Mn cluster.[9,10]

^{1}H ENDOR. The proton hyperfine couplings to the Mn cluster are remarkably few; only four resolved couplings within 5 MHz, all of which are associated with sites that are exchangeable with water. The qualitative conclusions from this are quite clear; there is no evidence for strongly coupled protons in the first coordination shell surrounding the Mn cluster and as few as two types in the second or third shells. These results point toward carboxylato type protein residues (Asp^- and Glu^-) as the predominant coordinating ligands to the Mn cluster. The γ-methylene hydrogens would be located at a distance that places them near the limit for resolved dipolar hyperfine interactions and, moreover, would be nonexchangeable with ^2H_2O. Protons with larger anisotropic coupling constants would not have been detectable in these ENDOR experiments owing to the limited sensitivity. Ligand ^{1}H hyperfine constants in a variety of $Mn^{III}Mn^{IV}$ model complexes all fall below 9 MHz. Larger hyperfine couplings might be resolved by EPR spectroscopy. The multiline EPR spectrum exhibits unresolved substructure of unknown origin. This is insensitive to ^2H_2O exchange and so rules out labile protons with large hyperfine couplings.

Table IV. ^{1}H ENDOR Hyperfine Constants (MHz) of $Mn^{III}Mn^{IV}$ Complexes

signal origin	peak position									ref
	a	b	c	d	e	f	g	h	i	
1[a]	0.6[e]	1.5[e]	2.6[e]	3.9[e]	4.1[e]	4.5[e]	5.7[e]	6.8[e]	8.6[e]	22
2a[b]	1.0[e]	2.3[e]	4.7[e]	8.3[e]						23
2b[c]	1.1[d]	2.1[d]	2.8[d]	3.6[d]	4.9[d]	6.2[d]				23

[a] $(HBPz_3)Mn(\mu\text{-}O)_2(\mu\text{-}O_2CR)Mn(Pz_3BH)$; R = CH_3, $CD_3C_2H_5$ $C(C_6H_5)_3$. [b] $[(bpy)_2Mn(\mu\text{-}O)_2Mn(bpy)_2]^{3+}$ in bpy/bpy$^+$ buffer, pH = 4.6. [c] $[(bpy)_2Mn(\mu\text{-}O)_2Mn(bpy)_2]^{3+}$ in acetate buffer, pH = 4.6. [d] ^2H_2O exchangeable. [e] ^2H_2O nonexchangeable.

Kawamori et al. have reported proton ENDOR spectra attributed to the S_2 multiline signal in spinach PSII membranes.[5] Their results differ greatly from our data, suggesting the possibility of a significant difference in the proton coordination structure of the WOC between spinach and *Synechococcus*. As listed in Table II, they report six pairs of light induced resonances between 4 and 0.5 MHz, only two of which are exchangeable in ^2H_2O. We fail to see most of the couplings they report as due to the S_2 multiline signal, except for the pairs at 2.4 and possibly at 1.2 MHz (1.0 MHz our result). While we both observe the 2.4 MHz resonance to be exchangeable in ^2H_2O, we clearly differ on the exchangeability of the 1.0 MHz proton. They do not report the resonance we see at 4.9 MHz. We can observe a weak hyperfine splitting of 0.5 MHz which agrees with one which these authors report, but only if we subtract a Gaussian peak to account for the overlapping matrix peak. This peak is exchangeable with ^2H_2O in our experiments, while Kawamori report no exchange. The other resonances they report at 4.0, 1.4, 0.7 we also see, except they are not light induced and all three originate from the dark ENDOR spectrum of the Tyr-D$^+$ radical, as shown in Figure 4B2 and previously reported by Babcock et al.[29] We cannot distinguish the 0.5 MHz coupling from the matrix peak. Our assignments were established by the EIE experiment. We believe the assignments given by Kawamori et al. for the ENDOR resonances of the WOC in spinach are at least partly incorrect. We attribute this discrepancy to the high-temperature sensitivity of the ENDOR signal from the S_2 multiline and to interference by Tyr-D$^+$. We were unable to obtain reliable ENDOR data from the Mn cluster using a gaseous helium cryostat at 5–6 K, as used by these authors. For this reason all measurements reported in the present study were performed in liquid helium at 2.1 K. Also, in order to obtain distance information Kawamori et al. treat the Mn cluster as a point source of spin density and attribute the hyperfine interaction solely to dipolar coupling, ignoring the possibility of isotropic hyperfine coupling via the Fermi contact interaction. We show in a later section that these approximations lead to incorrect estimates of the proton coordinates.

^{1}H ENDOR of Model Complexes. Unfortunately, we found no literature reports on the hyperfine constants for imidazole protons bound to Mn^{III} or Mn^{IV} complexes. The proton hyperfine constants for two previously reported dimeric $Mn^{III}Mn^{IV}$ complexes are summarized in Table IV.[22,23] ENDOR was also measured

(26) Cooper, S. R.; Dismukes, G. C.; Klein, M. P.; Calvin, M. C. *J. Am. Chem. Soc.* **1978**, *100*, 7248–7252.
(27) Dikanov, s. A.; Tsevetkov, Yu. D.; Khangulov, S. V.; Goldfeld, M. G. *Doklady Biophysics* **1988**, *302*, 107–206 (Engl.).
(28) (a) Dismukes, G. C.; Ferris, K.; Watnick, P. *Photobiochem. Photobiophys.* **1982**, *3*, 243–248. (b) Dismukes, G. C. In Mixed Valency Systems: Applications in Chemistry, Physics and Biology; Prassides, K., Ed.; Kluwer Academic Press: 1991; NATO ASI, Vol. 343, pp 137–154.
(29) Chandrashekar, T. K.; O'Malley, P. J.; Rodriguez, I.; Babcock, G. T. *Photosyn. Res.* **1986**, *10*, 423–430.
(30) Peisach, J.; Mims, W. B.; Davis, J. L. *J. Biol. Chem.* **1979**, *254*, 12379–12389.
(31) Magliozzo, R. S.; Peisach, J. *Biochem.* **1992**, *31*, 189–199.

in CH_2Cl_2 and Cl_3CD solvents on the series of $Mn^{III}Mn^{IV}$ complexes with formula $[(HBPz_3)Mn(\mu\text{-}O)_2(\mu\text{-}O_2CR)Mn(Pz_3BH)]$, **1**, R = CH_3, CD_3, C_2H_5, $C(C_6H_5)_3$, as well as the isotopically exchanged B–D bond.[22] As many as 9 or 10 resolved proton couplings were found between 8.6 and 0.6 MHz. None were exchangeable in ^2H_2O. All of these couplings were found to arise from the three pyrazole ring protons. No resolved couplings from either the bridging carboxylates, or the terminal B–H bond nor from solvent were detected. Because the Mn ions exhibit trapped valences, there are at least four types of pyrazoles. Accordingly, at least 12 different pyrazole protons exist; more than enough to account for the 10 resolved couplings. ENDOR measurements of dimanganese(III,IV) complexes utilizing an aromatic pyridyl type ligand (TMPA) and a cyclic secondary amine (CYCLAM) also found ligand ^1H hyperfine interactions in the range 2.0–8.9 MHz.[24] To the extent that imidazole ligands to $Mn^{III}Mn^{IV}$ complexes may have similar ^1H hyperfine interactions, we can expect that imidazole could have proton couplings as large as 8.6 MHz, presumed to originate from the Mn^{III} ligands bound to σ coordination sites. We do not see such a large ^1H coupling constant in PSII, which is consistent with our assignment of the ^{15}N ENDOR results also indicating no σ type N donor ligands to Mn^{III}.

Imidazole proton hyperfine couplings for coordination to π sites on Mn^{III} or Mn^{IV} should be much smaller than for σ sites. The ^1H hyperfine constants reported for imidazole coordinated to the π site on low-spin $Fe^{III}(TPP)(Im)_2^+$ occur in the range which we observe for protons interacting with the WOC, (MHz): 3.5–3.7 (C-2), 1.2 (N-3), ~0 (C-4), and 2.7–4.8 (C-5).[25] Since these values are believed to be largely dipolar in nature,[25] we are unjustified in using the previous scaling by 2 S_z to estimate the Fermi contact hyperfine constants. If the hyperfine interaction is purely dipolar than the proper scaling factor to use to extrapolate these values to a spin-coupled $Mn^{III}Mn^{IV}$ center is $S_i \cdot S/S^2$. This could range anywhere from +2 to −1 depending on which Mn ion the proton is closest to.[23] If there is significant coupling to two Mn ions then the model used in the following section needs to be applied. Although the N-3 and possibly the acidic C-2 protons ought to be exchangeable with ^2H_2O for imidazole bound to Mn^{III} or Mn^{IV}, the C-4 and C-5 sites should not be. Since the C-4 imidazole site in the low-spin heme system exhibits no observable coupling and the C-5 site in histidine is bound to the β carbon rather than to a proton, we see that only two ring protons at N-1 and C-2 may be large enough to yield resolved hyperfine couplings. The β carbon protons ought to be close enough to have a dipolar interaction and should be nonexchangeable. This suggests that there ought to be three distinct protons each having as many as three hyperfine constants if full rhombic symmetry of the hyperfine tensors exists. This is far more complex a ^1H spectrum than we observe in PSII, where only four resolved splittings are found. So either the approximations used to make this extrapolation are incorrect or the histidine ligand hypothesis is not compatible with the proton ENDOR. More model studies (and stronger signals from the WOC) are needed to resolve this.

^1H Hyperfine Constants for Water Protons. To complete the discussion of relevant model complexes we summarize the proton couplings observed for $(bpy)_2Mn^{III}(\mu\text{-}O)_2Mn^{IV}(bpy)_2^{3+}$ in 50 mM bipyridine buffer, **2a**, and for the same compound in acetate buffer, **2b**.[23] Removal of bpy from the aqueous solution leads to dissociation of bpy ligands and replacement by acetate or water, as was followed by the disappearance of all of the ^{14}N ENDOR resonances from **2a**.[23] Ligand exchange leads to little change in the ^{55}Mn hyperfine constants and only a minor change in the EPR line width (not shown). Removal of bpy leads to the loss of all of the ^2H_2O nonexchangeable protons and their replacement by six hyperfine couplings in the range 1.1–6.2 MHz, all of which are now ^2H_2O exchangeable. Based on the analysis given in refs 22 and 23, these correspond to water molecules which are H-bonded either to μ-oxo bridges or to terminal acetate O atoms. This experimental result implies that the methyl protons from coordinated acetate ligands do not give resolved couplings, and so we can expect the protein Asp and Glu ligands would behave similarly. Surprisingly, **2a** exhibited no exchangeable protons, indicating that even in aqueous bpy buffer at pH 4.6 the oxo bridges ($pK_a < 2.5$) are blocked from forming strong H-bonds to the solvent. The predicted dipolar hyperfine constants for protons H-bonded to the oxo bridges should be quite large and easily detectable (see next section). The ^{14}N and ^1H ENDOR results suggest that most or all of the bpy ligands are displaced in concentrated acetate buffer at low pH.

Table V. PSII ^1H ENDOR Data Reduction into Scalar and Dipolar Hyperfine Constant (MHz)

obsd	case	1	2	3	4	simulation
$\|A_a\| = 5.0$	$A_a^{dip} =$	−4.5	−3.8	−2.9	−2.2	−4.6
$\|A_b\| = 2.4$	$A_b^{dip} =$	2.9	3.6	−0.3	0.4	+3.3
$\|A_c\| = 1.0$	$A_c^{dip} =$	1.5	0.2	3.1	1.8	+1.6
	$A_{scalar} =$	−0.53	−1.2	−2.1	−2.8	−0.6

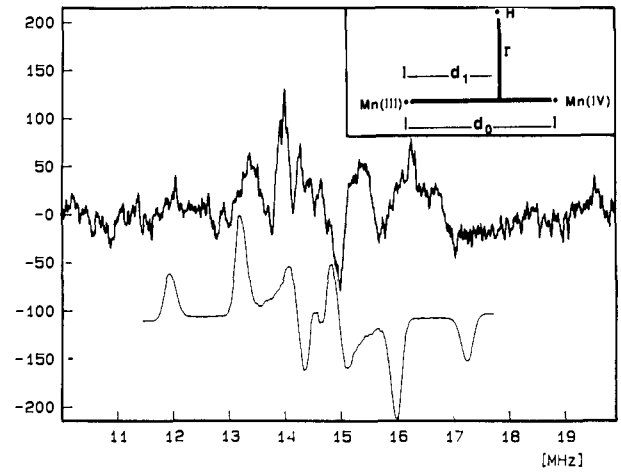

Figure 5. (Top) Light-minus-dark ^1H ENDOR signal from the S_2 multiline EPR signal in *Synechococcus el.* The spectrum differs from Figure 3C by subtraction of a central Gaussian peak equal in line width to the matrix peak. (Bottom) Simulated ^1H ENDOR signal using the "spin-coupled point pair" model described in the text.

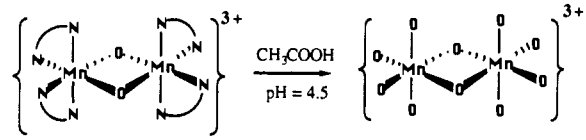

2a **2b**

Proton Coordinates from Hyperfine Constants for the WOC. Estimated values for the dipolar and isotropic hyperfine constants were obtained directly from the experimental spectrum by equating the sum of the three largest splittings to the trace of a single hyperfine tensor, $\sum_i A_i = 3A_{isotropic}$. Although this is a rigorous expression, it does assume that the three largest splittings originate from one class of protons. This is the simplest but not necessarily the only possibility. Because the signs of the splittings are not determined experimentally, this sum can be obtained in four possible ways, as noted in Table V, cases 1–4. Only one of these choices, case 1, gave approximate agreement with the dipolar and isotropic hyperfine constants deduced from spectral simulations (column 6, Table V). The three other sign choices could not be accounted for by locating a single proton at another site, and so these were rejected.

A theoretical model—the "spin-coupled point pair" model—which describes the hyperfine interaction between a ligand nucleus and a pair of spin-coupled paramagnetic ions was used to simulate the ^1H ENDOR spectrum.[23] This model predicts that a single rhombic hyperfine tensor approximately reproduces the ENDOR line shape for all three of the major hyperfine constants in the spectrum at 4.9, 2.4, and 1.0 MHz, as shown in Figure 5 (bottom) for the case of a proton interacting with an isolated $Mn^{IV}Mn^{III}$ pair in the $S = 1/2$ spin state. The parameters used for this

simulation were d_0 = 2.70 Å, d_1 = 1.35 Å, R = 3.8 Å, and A(iso) = −0.6 MHz. This site is located at a position very close to equidistant between the two Mn ions and along a perpendicular to the Mn–Mn vector (see insert to Figure 5). The smallest splitting of 0.5 MHz seen in the experimental trace in Figure 5 is quite weak and appears to originate from a second type of more distant proton which we will not discuss further. Because of the low S/N ratio of the current data the structural model must be considered tentative and primarily serves to illustrate only the simplest point-pair model. Other interpretations may be possible. Inclusion of spin transfer onto the μ-oxo atoms which bridge the Mn ions could either increase or decrease the predicted Mn–H distances in a manner which is difficult to predict, because either α or β spin density could be transferred. It is also clear that the metrical predictions would change significantly if the proton site(s) interact appreciably with all four Mn ions. We are pursuing studies aimed at examining these possibilities.

It is satisfying that the model which requires the fewest number of proton sites to explain the experimental data is also physically reasonable. It places a proton at R = 3.8 ± 0.1 Å. If we accept the picture derived from EXAFS studies that two μ-oxo atoms bridge between the Mn^{III} and Mn^{IV} ions,[32] then this corresponds to a minimal distance of 2.6 Å from the μ-oxo atoms, assuming the proton is coplanar with the Mn_2O unit. Such a long distance indicates an extremely weak H-bond. The number of equivalent protons in this class is not determined by the ENDOR experiment. The −0.6 MHz isotropic hyperfine constant obtained from the simulation is very small. It is comparable to the value for water molecules bound to Mn(II) in solution and much less than the predicted value for water bound to Mn(III) or Mn(IV).[33] The latter oxidation states are those found for manganese in the S_2 oxidation state in PSII. This small isotropic coupling in PSII suggests that this may not originate from a water molecule or hydroxyl ion directly bound to the Mn cluster. This hypothesis can be tested with model complexes in the future.

The proton coordinates obtained from this simulation were derived from what we consider to be the simplest reasonable model for analysis of the experimental data. The same conceptual model has been found to explain well the ^{1}H hyperfine data for the spin-coupled dimanganese(III,IV) state of catalase from *T. thermophilus*, complex 1, and the mixed valent state of the di-iron(III,IV) active site of uteroferrin.[23]

At the present state of low sensitivity, the ^{1}H ENDOR results on PSII reveal the four hyperfine constants noted in Table II. If there are undetected hyperfine interactions present, then they would have to be larger and more anisotropic than those in Table II to account for their absence in the ENDOR spectrum. Such large couplings should have appeared in the EPR spectrum, yet no ^2H_2O exchangeable features have been reported, despite attempts in several laboratories (except ref 3b). Also, no large ^{1}H couplings were observed in any of the model complexes possessing the Mn_2O_2 or Mn_2O cores with carboxylato, bipyridine, or pyrazolyl ligands. Thus, both the dipolar and isotropic hyperfine data suggest that there are no protons from directly coordinated water or hydroxo ligands to the Mn cluster. We reach the surprising conclusion that the active site of the water oxidase is comparatively "dry". By this, we mean that all water ligands bound directly to Mn atoms in the S_2 oxidation state must exist as fully deprotonated oxo atoms or be excluded from approaching closer than 3.3 Å. This seems to be a reasonable way to insure a high oxidation potential for the Mn cluster—through exclusion of *excess* water which would otherwise greatly stabilize the higher oxidation states of manganese. In this context, the role of calcium in the WOC has been found to involve the exclusion of excess water from the Mn_4 cluster.[16] This conclusion is consistent with the presence of the $(\mu\text{-O})_2$ bridging ligand structure between pairs of Mn ions in the WOC as suggested by EXAFS results.[32]

The ^{1}H ENDOR spectrum of the S_2 oxidation state of the WOC is very similar to that observed for the dimanganese(III,IV) oxidation state of catalase.[23] The simplicity of the spectra reveal limited accessibility of solvent (and presumably substrate) and thus a coordination environment determined largely by protein ligands. These ligands are predominantly carboxylato type in both enzymes. As many as two types of π-nitrogen ligands to the WOC can be detected by ^{15}N ENDOR and one π-type to Mn catalase by ^{14}N ESEEM.[27] The strong preference for carboxylato instead of nitrogen ligands distinguishes these enzymes from other dimetalloenzymes like hemerthyrin and hemocyanin where polyhistidine coordination prevails. The anionic carboxylate ligand should stabilize the higher oxidation states, accounting for the accessibility of multiple oxidation states in the manganese enzymes. By contrast, polyhistidine coordination stabilizes the reduced Fe^{II} oxidation state which is essential for reversible O_2 binding in hemerthyrin as well as the Mn^{II} oxidation state in the functionally inactive substituted myohemerthyrin (Kurtz, D. private communication).

Acknowledgment. We are grateful to Drs. S. Khangulov and M. Baumgarten and Mr. M. Zheng for permission to use their unpublished results. We thank John Marino for cells grown on [^{15}N]-nitrate. This work was supported by NIH Grant GM39932.

Supplementary Material Available: Figures S1A, S1B, and S1B-S1A, EPR dark, light and light-dark spectra for Figure 3, Figures S2A, S2B, and S2B-S2A, ENDOR dark, light and light-dark spectra for the ^2H_2O exchanged sample in Figure 3D, Figures, S3A, S3B, and S3B-S3A, ENDOR dark, light and light-dark spectra for the natural abundance ^{14}N spectrum related to Figure 2C, Figures S4A, S4B, and S4B-S4A, integrated EPR signals for dark, light and light-dark spectra for Figure 4Be, and Figures S5A, S5B, and S5B-S5A, ENDOR dark, light and light-dark spectra for the ^{15}N enriched sample in Figure 2A (15 pages). Ordering information is given on any current masthead page.

(32) (a) Guiles, R. D.; Zimmermann, J. L.; McDermott, A. E.; Yachandra, V. K.; Cole, J. L.; Dexheimer, S. L.; Britt, R. D.; Wieghardt, K.; Bossek, U.; Sauer, K.; Klein, M. P. *Biochem.* **1990**, *29*, 471–485. (b) Guiles, R. D.; Yachandra, V. K.; McDermott, A. E.; Cole, J. L.; Dexheimer, S. L.; Britt, R. D.; Bossek, U.; Sauer, K.; Klein, M. P. *Biochem.* **1990**, *29*, 486–496. (c) George, G. N.; Prince, R. C.; Cramer, S. C. *Science* **1989**, *243*, 789–791. (d) Penner-Hahn, J. E.; Fronko, R. M.; Pecoraro, V. L.; Yocum, C. F.; Betts, S. D.; Bolby, N. R. *J. Amer. Chem. Soc.* **1990**, *112*, 2549–2557.

(33) Sivaraja, M.; Stouch, T. R.; Dismukes, G. C. *J. Am. Chem. Soc.* **1992**, *114*, 9600–9602.